

A NUMERICAL SIMULATION OF CRUSHING IN FLEXIBLE PIPES

Alfredo Gay Neto, alfredo.neto@gmail.com

Clóvis de Arruda Martins, cmartins@usp.br

Celso Pupo Pesce, ceppesce@usp.br

Escola Politécnica, Life&MO - Offshore Mechanics Laboratory, University of São Paulo

Teofilo Barbosa Ferreira, teofilo.barbosa@prysmian.com

Prysmian Cables and Systems

Abstract. Flexible pipes are subjected to compressive loading when they are being launched. A set of shoes working together in the launching mechanism compress a region of the pipe in order to provide enough friction for sustaining its own weight during launching. This loading should be applied carefully, once the pipe may not change plastically its shape during installation, once residual ovalization can reduce the depth limit of pipe application. A restricted 3D numerical model is performed for a carcass profile example. Deformation shape and stresses are obtained, using a strain hardening material assumption, geometric nonlinear behavior and carcass internal nonlinear contacts. The presented model shows carcass stresses and displacements when subjected to crushing load. Carcass diametral variation values obtained in simulation are compared to experimental results.

Keywords: offshore engineering, flexible pipe, crushing

1. INTRODUCTION

Flexible pipes are composed by many layers, with different structural and operational functions. These layers are usually made of different materials, including metal and plastic. Each metallic layer has some structural functions, briefly described in the following items:

- Interlocked carcass (Figure 1): the innermost layer. Its operational function is conveying oil and gas flows. It must prevent the collapse due to the external pressure when the pipe outer sheath is damaged;
- Pressure armor layer: located between tensile armor layers and interlocked carcass, it is designed to resist both to internal and external pressure loads;
- Tensile armor layers: the outermost layer, which provides axial rigidity to the flexible pipe and contributes to pipe resistance to burst, increasing its radial stiffness.

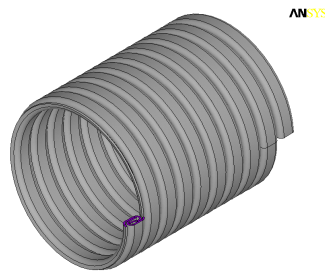


Figure 1 – Typical interlocked carcass geometry

Plastic layers on the tube provide water-tightness and also transmit pressure between the metal layers. Usually, one plastic layer is located between the interlocked carcass and the pressure armor layer, and another as an external sheath.

One important situation occurs when a structural failure happens on the external plastic layer. In this case, the external pressure loads the carcass layer, which must withstand this loading with no failure. This situation is critical, and undesired, but the carcass layer design must take into account this extreme loading condition. Gay Neto and Martins (2009) and Nogueira (2008) studied this situation.

When the pressure armor layer is present, it acts as an important structural element, providing stiffness in radial direction for the flexible pipe as a whole. In normal operational situation, the pressure armor layer and the tension armor layer support together the internal pressure of the pipe. The internal fluid pressure is not supported directly by the interlocked carcass, as it does not provide tightness.

This work deals with a situation that occurs during the flexible pipe installation. This will be more detailed in the next section.

2. FLEXIBLE PIPE INSTALLATION

Installation is a critical situation for a flexible pipe. It is an extreme loading situation in which structural failure can occur. Installation ships provide the necessary equipment for sustaining flexible pipes during installation. Equipment includes a set of shoes that press directly the external sheath of a flexible pipe, keeping it fixed to the vessel through friction. The purpose of this lateral pressure applied to flexible pipes is to increase the normal loading, providing more friction availability for flexible pipe sustaining. An example of installation ship is shown in Figure 2.



Figure 2 – An example of installation ship – extracted from Technip (2000)

A schematic illustration of the shoes action is presented in Figure 3. One can see that the flexible pipe passes through a launching wheel, hung at one side and fixed by shoes at the other side. There are very important effects that need special attention in flexible pipe installation. One remarkable loading situation in installation is related to the flexible pipe passage by the launching wheel. The flexible pipe can present significant ovalization, depending on the curvature radius of the launching wheel and on the tension level in the flexible pipe hanging portion. The present work does not deal with this problem.

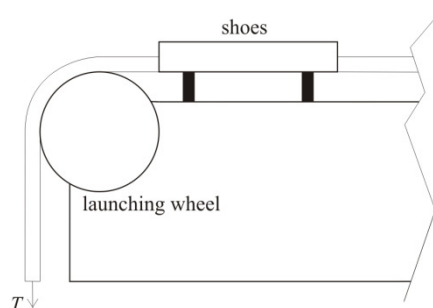


Figure 3 – Scheme of shoes action that provides flexible pipe sustaining during installation (T is the tension on flexible pipe hanging portion)

This work deals specifically with the shoes region, where the flexible pipe can be subjected to external loading. The shoes get in contact with the external sheath of the flexible pipe, applying on it a large value of pressure, in order to increase normal component of contact force (and also increasing the friction level available for flexible pipe tension equilibrium). Depending on shoes loading magnitude, the flexible pipe can crush. It is undesirable, once a crushed flexible pipe has its external pressure work value decreased when compared to the uncrushed one; see, e.g., Gay Neto and Martins (2009). It is very important to present a numerical study of crushing situation, in order to predict the maximum level of loading that the installation ship equipment may act, with no important crushing applied to the flexible pipe. As pointed out by Sousa et al. (2001), one of the challenges for installing flexible pipes in ultra deep water is the increasing in installation loads necessities for that. Then, a stress prediction for installation loading on flexible pipes is necessary. Sousa et al. (2001) still point out that the two most important installation loads are the pipe weight and the crushing loading applied by the shoes of installation ship.

The case study considered in this paper is critical: a flexible pipe that does not contain the pressure armor layer. In this kind of flexible pipe, carcass layer receives almost all loading from shoes. In order to model carcass layer behavior a 3D Restricted Model was used in this work. This model was presented in Gay Neto and Martins (2009), and used to study the interlocked carcass behavior, when this layer is loaded by an external constant pressure on its external surface. Authors present the carcass 3D Restricted Model compared to other models, including comparisons with a Full 3D and with an Analytical Model.

Basically, this 3D model considers the carcass layer as a ring, and not a helix, as it is in reality. However it is expected that for crushing situation this assumption does not affect significantly the results. Gay Neto and Martins (2009) showed that for external pressure loading on carcass, the pitch effect may be neglected when studying carcass collapse. When this geometrical simplification is made the problem becomes simpler and present geometrical symmetries, providing better quality meshes with not so much computational cost as it would occur when dealing with a Full 3D Model.

Martins et al. (2003) still show a carcass layer study during launching. They present an analytical model for calculating carcass behavior, when subjected to various loading situations such as 2 forces, 3 forces, 4 forces or external pressure. The model expands radial loading as a Fourier series and its results are compared to experimental data, showing its range of application. In linear region of loading the proposed model showed excellent results, but out of linear range did not, as it should be expected. The authors define a loading parameter λ related to the carcass behavior during launching:

$$\lambda = \frac{Pa^2}{\pi ei} \quad (1)$$

In which:

- P is the shoe loading, applied to a sample of flexible pipe carcass;
- a is the inner radius of carcass;
- ei is the minimum inertia moment, per unit length of carcass. Its value can be calculated using Young Modulus of carcass material and the minimum moment of inertia, as mentioned in Gay Neto and Martins (2009).

Martins et al. (2003) concluded that there is an upper bound to a stiffness changing in structure for this loading coefficient: $\lambda = 3$ and Gay Neto and Martins (2009) still point this out through a different methodology. This is a representative value of buckling on this kind of structure, considering it ideally, without imperfections. For a distributed pressure loading on all external surface, this value represents the numerical order of the real carcass expected buckling behavior. However, buckling conditions are dependent on how are the forces really applied, if by 2 forces, 3 forces, or through a uniform pressure. For the crushing problem with 2 forces, for example, Martins et al. (2003) notice a change in linearity about $\lambda = 0.1$ in the experimental result for the considered carcass profile. After this value of λ , crush behavior changes and the structure becomes less stiff.

Sousa et al. (2001) show a very complete finite element model of flexible pipes, containing all layers and considering the carcass and pressure layers as equivalent pipes, using first order shell elements, with 6 degrees of freedom for each node. A crushing analysis is performed and compared to experimental results. The experiment is made with a three shoes equipment, and results show a curve qualitative similar to the presented results in this work.

3. FINITE ELEMENT MODEL

For predicting the order of the collapse loading to be imposed during experiment, a finite element analysis was constructed, trying to represent the exactly conditions to be physically tested. Figure 4 shows the geometrical model.

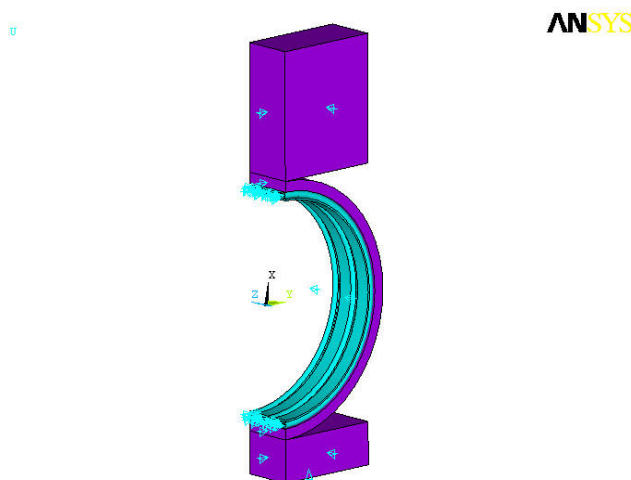


Figure 4 – Geometric model considered and its boundary conditions

Geometric model contains the interlocked carcass and the plastic layer. The carcass profile used for these simulations is shown on Figure 5 and its relevant properties on Table 1.

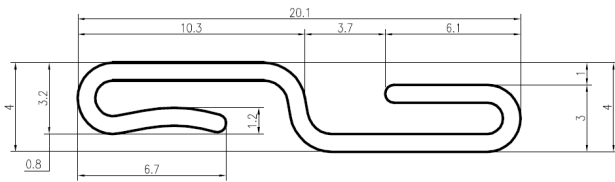


Figure 5 – Carcass profile (measures in mm)

Table 1 - Carcass layer general properties

Internal Diameter	4.0"
Material Young Modulus	193 GPa
Material Poisson ratio	0.3
Thickness of profile ribbon	0.8 mm

One can note that the pitch of the carcass was neglected. This procedure tries to simplify the FEM model, introducing some symmetry that does not occur in the real problem. By this procedure, it is possible to perform an analysis using a half model as shown on Figure 4.

Looking the geometry it is possible to see two large blocks in the extreme sides of the internal plastic layer. Their function is to represent the shoes, which movement is imposed along the radial direction of carcass, performing the crushing situation.

A totally mapped mesh was constructed based on the geometry; see Figure 6. Representing the problem domain, first order solid elements were used (SOLID185) This element has 8 nodes in its original shape, but can be degenerated to prisms (6 nodes) or tetrahedral (4 nodes). The degrees of freedom considered for each node are the displacements, in x , y and z directions. A detailed element formulation description can be found in Ansys help (2009). Both the carcass layer and internal plastic layer were represented using the same element kind. Mesh contains 153,263 nodes, each one with 3 degrees of freedom. Both the blocks, considered to represent the upper and lower shoes, are meshed, each one with just one single element. This choice will be explained in the contacts and boundary conditions section.

First order elements are a good choice for this study, because they are better than second order elements for dealing with contact regions. Four divisions in ribbon thickness direction were considered in the carcass mesh, what would be enough for representing well the stress gradient in this direction, using first order polynomials as shape functions.

One can observe that the plastic layer mesh is coarser than the carcass one. This was done because the objective of this work is to study the carcass layer behavior, and the polymeric layer act just transferring the load. One known fact that can occur in reality, but is not captured using the proposed mesh for the polymeric layer, is the polymer extrusion. Plastic layer can penetrate the carcass voids when subjected to an external pressure. This phenomenon modeling is not the aim of this study. As a loading transfer, polymeric layer is well modeled with the mesh shown in Figure 6.

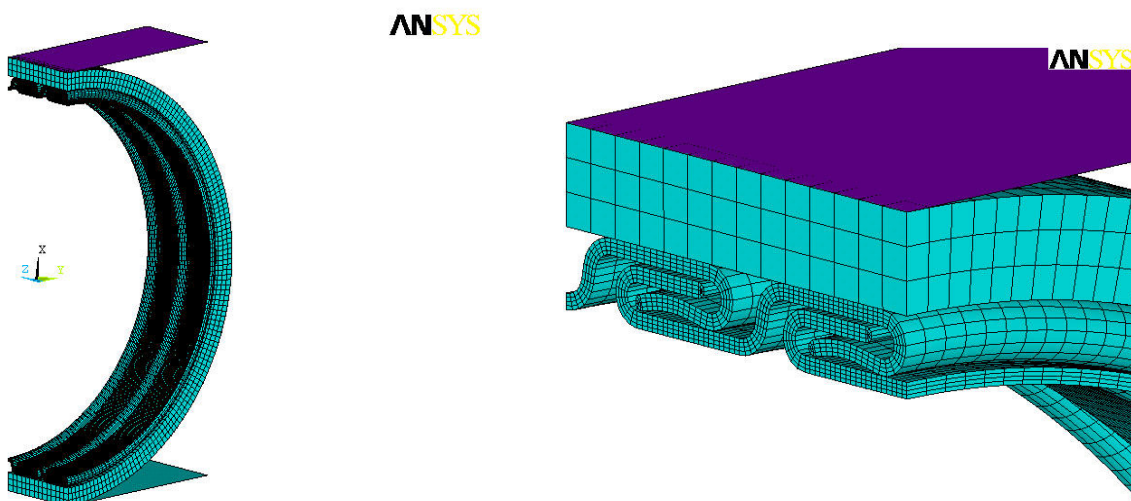


Figure 6 - (a) Mesh used in simulation (b) Detail of mesh

4. BOUNDARY CONDITIONS AND CONTACTS

The boundary conditions considered include some displacement impositions, directly acting on degrees of freedom of the problem. Values of x direction displacements are imposed on the upper face of the larger block, step by step, as in

the experiment. One alternative procedure would be to impose the forces and get the displacements as results. Numerical convergence using the Newton-Raphson Method is more difficult in the last option than in the first one. The first option was chosen for the model. In both options, the lower block is totally fixed.

The carcass layer and the internal plastic layer present symmetric boundary conditions at the region of the symmetry plane. Furthermore, one node of the carcass and another of the plastic layer were considered fixed in z direction, in order to avoid some rigid body motion. All boundary conditions are shown in Figure 4.

The two blocks (representing the shoes) are supposed to be in contact with the external surface of the polymeric layer. This contact aims at applying a 2 forces-condition in the carcass. Shoes are treated as *target* in ANSYS contact models, and the polymeric layer, as *contact*. The ANSYS Penalty Method contact algorithm used in these contact regions treats the contact physical phenomenon as a unilateral constraint. *Contact* and *target* (forming the contact pair) need to be defined carefully. The contact model constraint is: "The *contact* detection points are not allowed to entry the *target* region". Gauss integration points were considered in this model as the contact detection points. Due to that, a more refined mesh was used in the plastic layer than in the shoes (in order to create a large amount of Gauss points), and this mesh was defined as "*contact*". However, one single element was considered in the lower and in the upper block (defined as "*target*"). This procedure is similar to considering the blocks as rigid bodies (that would be a modeling option, too). These contact pairs were considered as frictionless.

Contact between the polymeric layer and the external carcass layer surface was also considered, for loading transferring purposes. The contact formulation for this pair uses the Penalty Method and its behavior is frictionless.

One can see in Figure 4 that two carcass rings were considered in this model but the ring behavior enforces a kinematic coupling in the considered cutting regions (parallel to xy plane). For considering this coupling correctly, the conditions shown in Figure 7 were taken. Such conditions include all displacements directions for the coupled nodes.

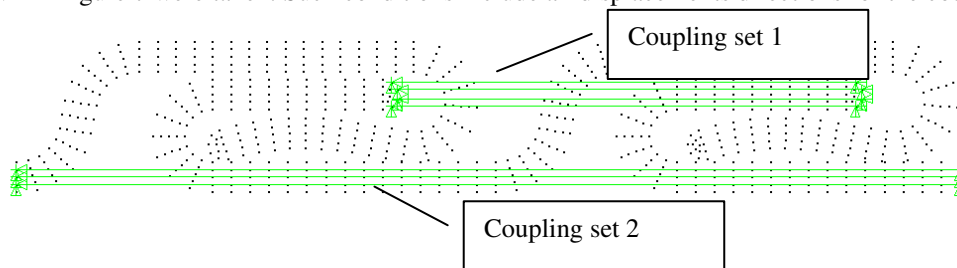


Figure 7 – Coupling sets considered in 3D Restricted Model

Nonlinear contact pairs in the internal surfaces of the carcass layer were considered in the model. These pairs are shown in Figure 8. The elements used for considering the contacts are CONTA174 and TARGE170. Basically, CONTA174 defines some contact detection points that are constrained to penetrate a region defined by TARGE170. More details about the contact elements formulation are found in Ansys help (2009). The mathematical algorithm adopted in the case of CONTA174 detection points penetrating the TARGE170 regions is the Penalty Method, with penalty stiffness factor value equal to 0.1. Contact behavior is assumed to be frictionless. These contact parameters have shown to represent well the carcass physical behavior during its crushing.

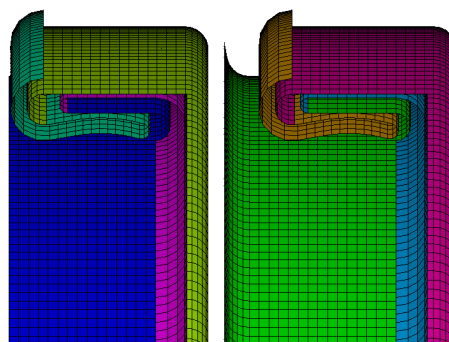


Figure 8 – Contact regions considered in the 3D Restricted Model

Furthermore, geometrical nonlinearities were considered, once the structure experiments large values of displacements. The stiffness matrix needs to be updated due to these displacements. Physical nonlinearities were considered too and are presented in next section through the adopted material curves.

5. MATERIAL PROPERTIES

Material data obtained from three repetitions of a uniaxial tension test in carcass layer steel is shown in Figure 9. Necking of the specimen was not achieved.

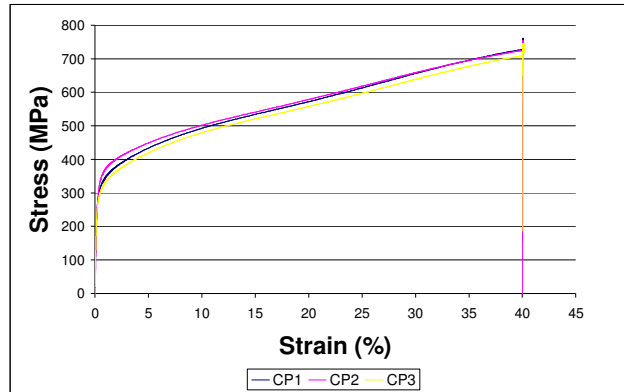


Figure 9 – Original material curve of carcass layer steel

Stresses and strains are given in this curve in engineering values. In order to input ANSYS data correctly, one needs to convert those values into real stresses and strains. The material property correction was determined as in Callister (2007),

$$\begin{aligned} \sigma_R &= \sigma_E(1 + \epsilon) \\ \epsilon_R &= \ln(1 + \epsilon) \end{aligned} \quad (2)$$

In these equations, σ_R is the real stress value related to an engineering stress value σ_E and to an engineering strain value ϵ , which is also related to a real strain ϵ_R .

Furthermore, an additional assumption was made about carcass manufacturing and its influence in material properties: a curve offset was made after converting with equations (2). In order to consider some hardening due to carcass manufacturing, material curve was shifted by 0.2% to the left, therefore emulating loading re-distribution beyond the plastic strain. The offset emulates the new conformed material behavior.

The aforementioned procedure results in the material curve shown in Figure 10.

Points of such a material curve are shown in Table 2. Young modulus was taken as 203,337.5 MPa and the Poisson ratio as 0.3. Plastic strain occurs beyond 285 MPa.

Von Mises plasticity with isotropic hardening was considered in the material curve of Figure 10 for ANSYS simulation. This kind of hardening rule is convenient for large strain simulations and non repetitive loading.

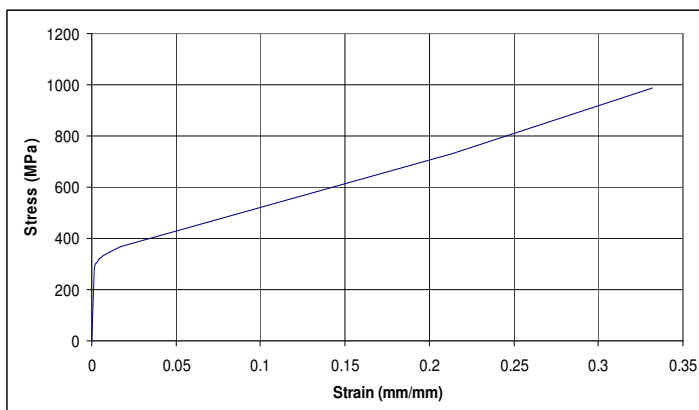


Figure 10 – Material curve of carcass layer steel

Table 2 – Material curve points of carcass layer steel

Strain (mm/mm)	Stress (MPa)
0.00000	0
0.00140	285
0.00236	299
0.00319	307
0.00448	319
0.00520	323
0.00632	330
0.00873	341
0.01068	349
0.01697	370
0.21349	731
0.33215	988

For the plastic layer, a multi-linear elastic material model was taken. No plasticity was modeled. Material curve is shown in Figure 11 and the corresponding points in Table 3. Young modulus is 490 MPa (for small strains) and Poisson ratio is 0.45.

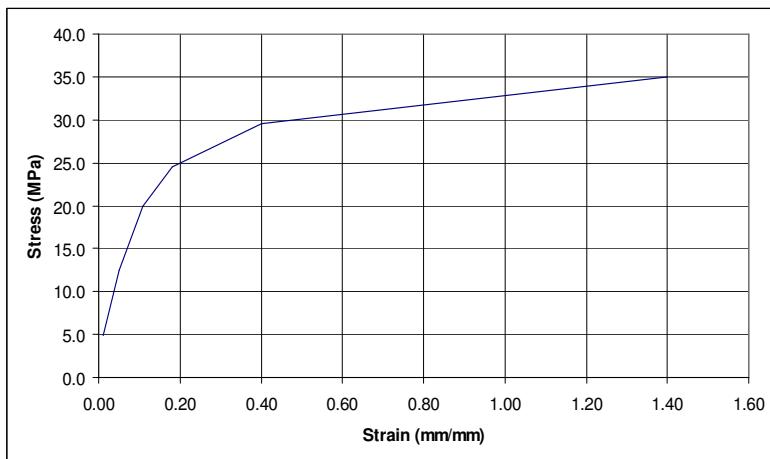


Figure 11 – Material curve of plastic layer material

Table 3 – Material curve points of plastic layer material

Strain (mm/mm)	Stress (MPa)
0.00	0.0
0.01	4.9
0.05	12.5
0.11	20.0
0.18	24.5
0.40	29.5
1.40	35.0

6. EXPERIMENT

An experimental procedure was performed, in order to validate the numerical model. The experimental apparatus apply the same boundary conditions and loading as in the numerical model. Apparatus is schematically shown in Figure 12.

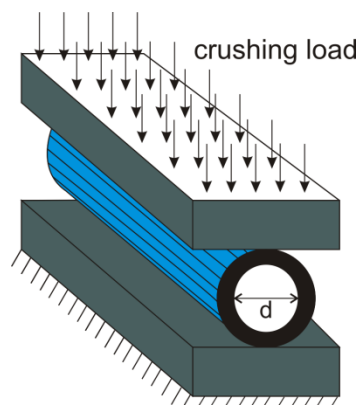


Figure 12 – Experimental apparatus (schematic)

A crushing load is applied in the upper block and the internal flexible pipe diameter value is measured in the indicated direction (horizontal). Its variation indicates the ovalization, due to crushing.

7. NUMERICAL RESULTS

Results show the horizontal diameter variation of carcass *versus* the load applied by the upper block. The value of the applied load is calculated as a reaction load in the degrees of freedom which are constrained in *x* direction. Results are plotted for two different values of carcass diameter (4" and 2.5").

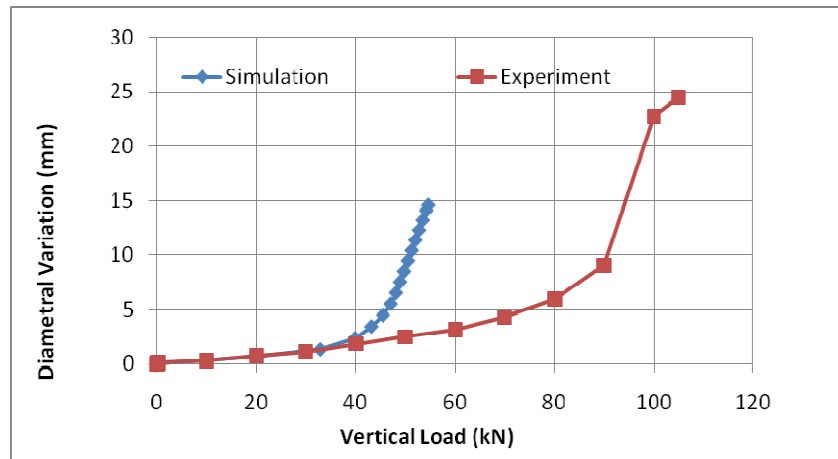


Figure 13 – 2.5” diameter carcass results (for a 750.5 mm length carcass)

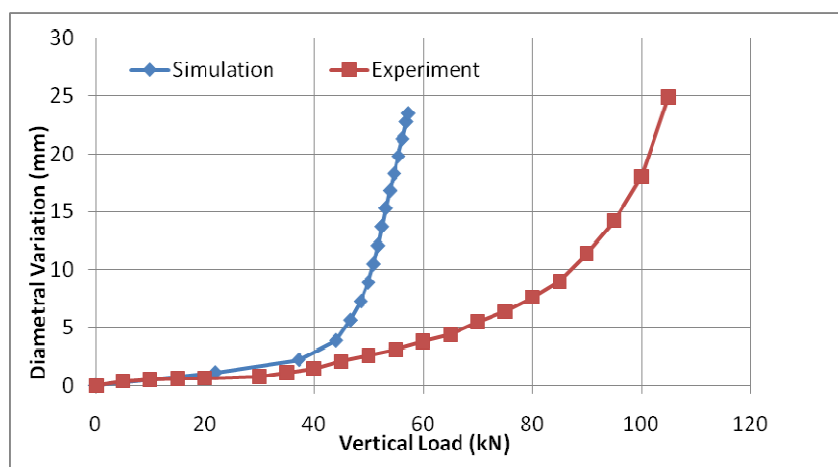


Figure 14 – 4.0” diameter carcass results (for a 742.5 mm length carcass)

Both results show that, for the considered carcass profile, the value of the load parameter related to linearity change is approximately $\lambda = 0.06$. Results shown by Martins et al. (2003) are somewhat different, though of same order of magnitude, once for that profile linearity was lost at $\lambda = 0.1$. Displacements related to the end points (larger loading value) of both curves (Figure 13 and Figure 14) are shown in Figure 15.

Comparing the numerical model results and the experimental results, one can conclude that they had a very good correlation up to the end of linearity. Beyond that, numerical model results differ from the experimental ones. Simulation starts changing its linearity due to the changes in the carcass layer metal properties, when plastic strain occurs. Additionally, geometric nonlinearity also occurs. The numerical model showed to be conservative, once the strength loss occurred before than in the experiment. The experimental stiffness change is smoother than in the simulation.

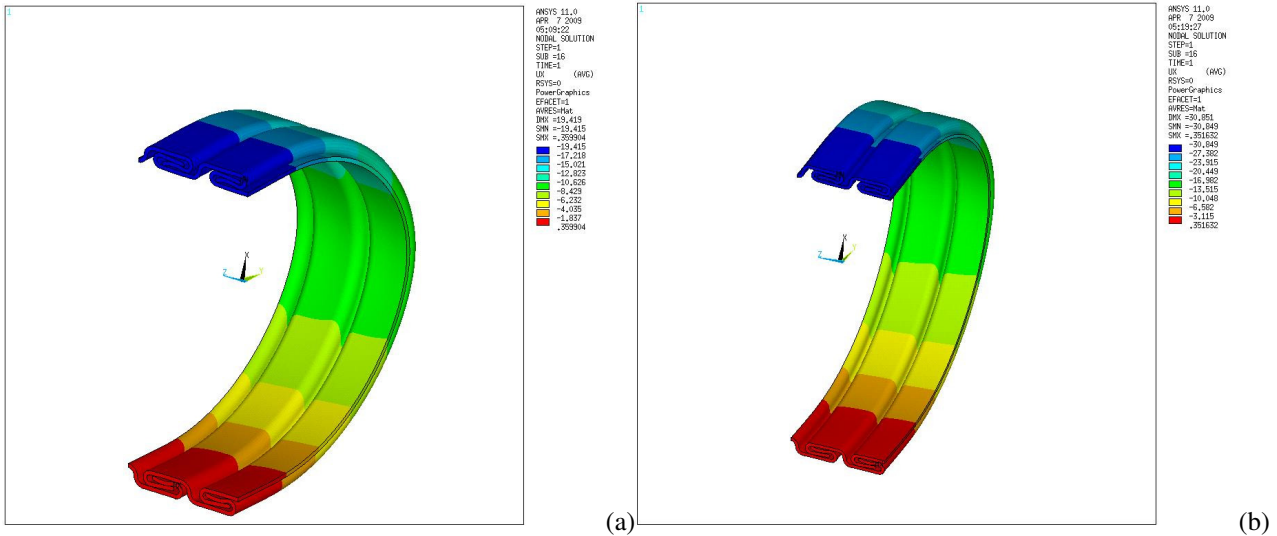


Figure 15 – Displacements field in x direction at end points of crush curves
 (a) 2.5''carcass (b) 4''carcass

Focusing on stress analysis, it is possible to see that for both carcass sizes, stress values at $\lambda = 0.06$ denote plastic behavior. Figure 16 shows von Mises stress field at this loading value. Increasing the crushing load on the carcass beyond this point, plastic strain spreads to a neighborhood of its initial values and the force necessary for crushing tends to saturate with a large displacement variation (this can be observed in curves shown on Figure 13 and Figure 14).

Plastic joints occur initially at top and bottom and, after a more pronounced loading at left and right points, as one can see in von Mises stress field distribution (Figure 17) which is related to the end points (larger loading value) of curves shown in Figure 13 and Figure 14.

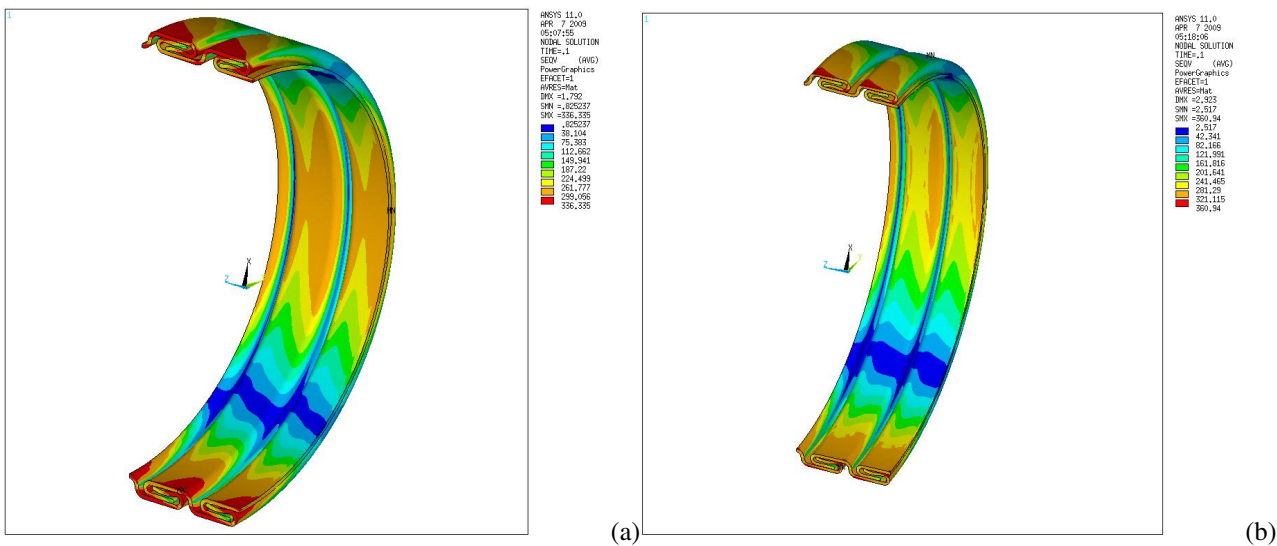


Figure 16 – Von Mises stress field at λ approximately 0.06
 (a) 2.5''carcass (b) 4''carcass

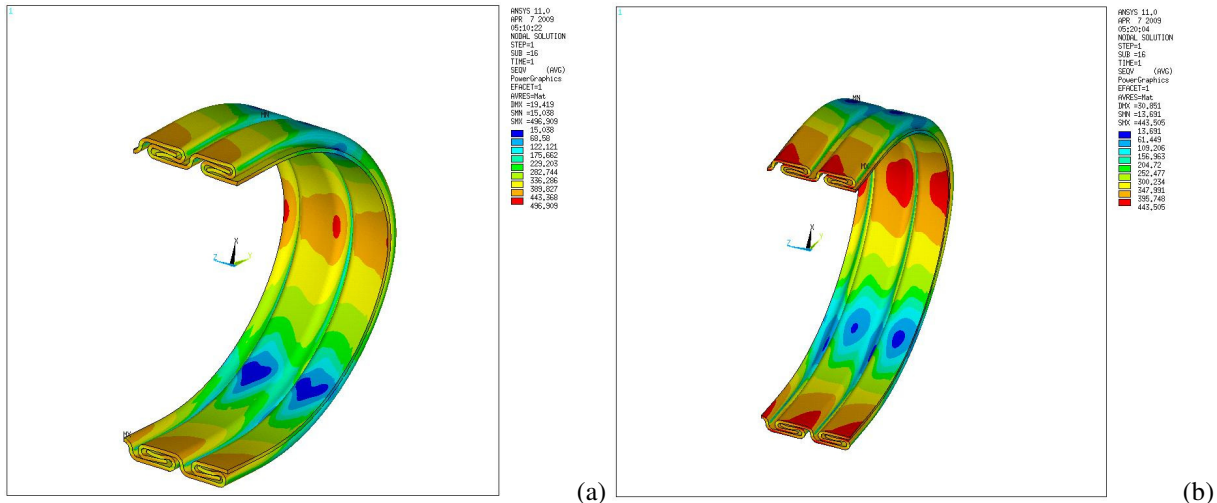


Figure 17 – Von Mises stress field at end points of crush curves
 (a) 2.5”carcass (b) 4”carcass

8. CONCLUSION

Results show that up to some vertical load applied by the upper block, a linear relation between force and radial displacement occurs. Such a result was likewise obtained in the numerical model and in the experiment. The linear regime slope in both curves agreed very well. Behavior changes when some plastic strain occurs, decreasing the stiffness of the carcass, with the appearance of plastic joints. The changing in the experimental stiffness occurs for larger values of loading than in the numerical model. An incorrect material behavior assumption could explain such a result. Since the carcass layer is manufactured through a metal forming process, strain hardening may not be neglected. The strain hardening behavior modeling for sure deserves further analysis.

The present numerical results served as a first prediction of the expected experimental results for a crushing test. The stress distribution field analysis shows quite clearly the importance of considering nonlinear material behavior modeling for the prediction of a crushed structure configuration beyond the linear regime.

9. ACKNOWLEDGEMENTS

The first author acknowledges FAPESP for funding his PhD studies under grant number 2006/06277-0.

10. REFERENCES

- ANSYS Inc; Ansys help. Release 12.0, 2009.
- CALLISTER JR, W.D.; *Materials Science and Engineering - An Introduction*. John Wiley & Sons, Inc. New York, 2007.
- GAY NETO, A.; MARTINS, C.A. *A comparative buckling study for the carcass layer of flexible pipes*. Proceeding of the 28th International Conference on Offshore Mechanics and Arctic Engineering, 2009.
- MARTINS, C.A.; PESCE, C.P.; ARANHA, J.A.P. *Structural Behavior of flexible pipe carcass during launching*. Proceedings of 22th International Conference on Offshore Mechanics and Arctic Engineering, 2003.
- NOGUEIRA, V.P.P.; *Análises Numéricas de Dutos Flexíveis Íntegros e Danificados sob Pressão Externa*. MSc. Dissertation (in Portuguese). Rio de Janeiro, Brazil, 2008.
- SOUSA, J.R.M., ELLWÄNGER, G.B., LIMA, E.C.P., PAPALEO, A.; *Local Mechanical Behavior of Flexible Pipes Subjected to Installation Loads*. Proceedings of 20th International Conference on Offshore Mechanics and Arctic Engineering, 2001.
- TECHNIP; *Sunrise*. Catalogue, 2000.

11. RESPONSIBILITY NOTICE

The authors are the only responsible for the printed material included in this paper.